Journal of Neurochemistry, 2005, **95**, 111–124 doi:10.1111/j.1471-4159.2005.03347.x

Lateral entorhinal cortex lesions rearrange afferents, glutamate receptors, increase seizure latency and suppress seizure-induced c-*fos* expression in the hippocampus of adult rat

Zsolt Kopniczky,* Endre Dobó,†,§ Sándor Borbély,‡ Ildikó Világi,‡ László Détári,‡ Beáta Krisztin-Péva,† Andrea Bagosi,† Elek Molnár§,[1] and András Mihály†,§,[1]

*Departments of *Neurosurgery and †Anatomy, Faculty of Medicine, University of Szeged, Szeged, Hungary*
‡Department of Comparative Physiology and Neurobiology, ELTE University, Budapest, Hungary
§MRC Centre for Synaptic Plasticity, Department of Anatomy, University of Bristol, School of Medical Sciences, Bristol, UK

Abstract

The entorhinal cortex (EC) provides the predominant excitatory drive to the hippocampal CA1 and subicular neurones in chronic epilepsy. Here we analysed the effects of one-sided lateral EC (LEC) and temporoammonic (alvear) path lesion on the development and properties of 4-aminopyridine-induced seizures. Electroencephalography (EEG) analysis of freely moving rats identified that the lesion increased the latency of the hippocampal seizure significantly and decreased the number of brief convulsions. Seizure-induced neuronal c-*fos* expression was reduced in every hippocampal area following LEC lesion. Immunocytochemical analysis 40 days after the ablation of the LEC identified sprouting of cholinergic and calretinin-containing axons into the dentate molecular layer. Region and subunit specific changes in the expression of ionotropic glutamate receptors (iGluRs) were identified. Although the total amount of AMPA receptor subunits remained unchanged, GluR1$_{flop}$ displayed a significant decrease in the CA1 region. An increase in NR1 and NR2B *N*-methyl-D-aspartate (NMDA) receptor subunits and KA-2 kainate receptor subunit was identified in the deafferented layers of the hippocampus. These results further emphasize the importance of the lateral entorhinal area in the spread and regulation of hippocampal seizures and highlight the potential role of the rewiring of afferents and rearrangement of iGluRs in the dentate gyrus in hippocampal convulsive activity.

Keywords: 4-aminopyridine, c-*fos*, entorhinal cortex, hippocampus, seizure, sprouting.
J. Neurochem. (2005) **95,** 111–124.

The entorhinal cortex (EC) receives strong afferentation from sensory association cortices, which project to layers II/III of the EC through the perirhinal and postrhinal areas (Swanson and Köhler 1986; Burwell and Amaral 1998; Witter *et al*. 2000). The polysensory information to the lateral and medial EC (LEC and MEC) is projected to the hippocampus by the lateral and medial perforant pathways, and temporoammonic (or alvear) path, innervating the molecular layer of the dentate gyrus, the stratum lacunosum-moleculare of the CA3, CA1, the subiculum, and the stratum oriens of the regio superior, respectively (Hjorth-Simonsen and Jeune 1972; Steward and Scoville 1976; Jones 1993; Witter *et al*. 2000). Most of the excitatory synaptic terminals of these pathways are glutamatergic (Mattson *et al*. 1988; Jones and Lambert 1990; Avoli *et al*. 2002). The rapid responses to glutamate at these synapses are mediated by postsynaptic AMPA, kainate and *N*-methyl-D-aspartate (NMDA) type ionotropic glutamate receptors (iGluRs) (Wisden *et al*. 2000). The EC also displays widespread, subcortical projections mainly to the amygdala, ventral striatum and the thalamus (Insausti *et al*. 1987). The important role of the EC in the pathophysiology of temporal

Received May 27, 2005; accepted June 1, 2005.

Address correspondence and reprint requests to Professor Elek Molnar, MRC Centre for Synaptic Plasticity, Department of Anatomy, University of Bristol, School of Medical Sciences, University Walk, Bristol BS8 1TD, UK. E-mail: Elek.Molnar@bristol.ac.uk
[1]These authors contributed equally to the intellectual input.

Abbreviations used: AChE, acetylcholinesterase; AMPA, α-amino-3-hydroxy-5-methyl-4-isoxazole-propionate; AOI, areas of interest; 4-AP, 4-aminopyridine; c-*fos*IR, c-*fos* immunoreactivity; DAB, 3′3′-diaminobenzidine tetrahydrochloride; EC, entorhinal cortex; EEG, electroencephalography; iGluR, ionotropic glutamate receptor; LEC, lateral entorhinal cortex; LECA, lateral entorhinal cortex ablation; MEC, medial entorhinal cortex; NMDA, *N*-methyl-D-aspartate; SOC, sham-operated control.

lobe epilepsy is reflected by its characteristic shrinkage, which is detectable with MRI on the side of the seizure focus in human (Reutens 1999). The neuropathological alterations of the epileptic EC are well known in the human and in experimental animals (Schwarz *et al*. 2000). However, it is not clear whether the neuronal loss in the EC is the cause or the consequence of the ongoing seizure process. There are also several questions as to the role of the EC in the precipitation, spread and maintenance of limbic seizure activity (reviewed in Avoli *et al*. 2002). The extrinsic and intrinsic connections of the MEC and LEC are well characterized (Burwell and Amaral 1998; Dolorfo and Amaral 1998; Kloosterman *et al*. 2000). The interlaminar EC connections and the electrophysiological properties of EC neurones are described in detail (Kloosterman *et al*. 2003). It was also demonstrated that reverberation of the seizure in MEC and LEC before its entry into the hippocampus is common (Iijima *et al*. 1996). This observation was verified in human, emphasizing the role of the EC and explaining why the MEC displays neuronal damage in long-lasting seizures (Bartolomei *et al*. 2005). However, the functional differences between the MEC and LEC concerning the precipitation and maintenance of the hippocampal convulsions are unclear. Detailed knowledge on the role of the EC–CA1 connections (the temporoammonic or alvear pathway; Raisman *et al*. 1965) in seizure is also lacking. Although it has a role in the maintenance of the seizure (Barbarosie *et al*. 2000), there are no anatomical data concerning the postsynaptic targets of this pathway in the regio superior. It has been proposed that the pathway mediates feed-forward inhibition, because its termination field is the stratum oriens, where the dendrites of perisomatic inhibitory cells and pyramidal cells are found (Freund and Buzsáki 1996). There are recent neurochemical data that support the role of the temporoammonic pathway in the mediation of feed-forward inhibition (Okada *et al*. 2004).

The significance of EC–hippocampal loops was further highlighted by *in vivo* experiments, where maximal dentate activation was abolished following EC lesions (Stringer and Lothman 1992). Others stressed the intrinsic properties of the hippocampus, proving that bilateral EC ablation did not eliminate epileptic afterdischarges in the hippocampal regions (Bragin *et al*. 1997). The destruction of the EC and the degeneration of the perforant path induce vigorous sprouting in the deafferented hippocampal layers (Deller and Frotscher 1997). The sprouting of cholinergic axons (Nadler *et al*. 1977), commissural calretinin-axons (Del Turco *et al*. 2003) and mossy fibers (Deller and Frotscher 1997) rearrange the synaptic connections of the dentate gyrus, the postsynaptic transmitter receptor populations and change the excitability of the hippocampus. Although the involvement of glutamate in the neuropathology of epilepsy is widely accepted (Sloviter 1983), only limited information is available about changes in iGluR subunit composition following EC lesion. The available EC lesion and perforant path transection studies used autoradiography to identify changes in AMPA, kainate and/or NMDA receptor ligand binding activities (Ułas *et al*. 1990a,b; Nicolle *et al*. 1997), or immunohistochemistry to investigate variations in some of the iGluR subunit proteins (Gazzaley *et al*. 1997; Mizukami *et al*. 1997; Adams *et al*. 2001; Iwakiri *et al*. 2002). Due to considerable variations in the experimental conditions used in previous studies, the cross-comparison of complex changes in different receptor and subunit types in individual hippocampal regions is difficult (see Discussion for details).

We have recently characterized the activity-dependent expression of the c-*fos* gene in cortical regions of the rat following 4-aminopyridine (4-AP)-induced seizures (Mihály *et al*. 1997, 2000, 2001, 2005). These studies indicate that c-*fos* induction in 4-AP seizure is mediated largely by iGluRs (Szakács *et al*. 2003), and c-*fos* transcription and translation (Fos mRNA and protein appearance in neurones) are tightly coupled processes (Mihály *et al*. 2005).

The aim of our present study was to investigate the effects of one-sided LEC and temporoammonic path lesion on: (i) 4-AP-induced seizure activity *in vivo*, (ii) acute experimental seizure-induced neuronal c-*fos* expression in the hippocampus, (iii) collateral sprouting in the deafferented hippocampal areas, and (iv) the expression and distribution of key iGluR subunit proteins. We found that cholinergic sprouting and the rearrangement of iGluR subunits are accompanied with a marked decrease in hippocampal seizure susceptibility. The lateral EC lesion was chosen, because the LEC is an important collector of polysensory information (Burwell and Amaral 1998) and seizure discharges (de Guzman *et al*. 2004) from the perirhinal and large neocortical areas.

Materials and methods

Entorhinal lesions

The experiments were conducted in accordance with prevailing laws and ethical considerations, according to the directive of the European Council (86/609 EEC) and to the Hungarian Animal Act. Specific approval was obtained in advance from the Faculty Ethical Committee on Animal Experiments (University of Szeged). Male Wistar rats (150–180 g) were anaesthetized with Calypsol® (100 mg/kg) plus atropine (0.01 mg/kg) given intraperitoneally (i.p.). The head of the animal was fixed in a stereotaxic frame, and following a vertical skin incision, the soft tissues and the temporalis muscle were cut in order to expose the temporal squama on the left side. The bone was cut with a dental drill, removed and the rhinal sulcus was identified. The cortical area inferior to the rhinal sulcus was electrocoagulated and suctioned (lateral entorhinal cortex ablation, LECA). The lesion of the LEC extended to all cortical layers and also the subcortical white matter, including the temporoammonic pathway, which originates from the MEC (Fig. 1; Raisman *et al*. 1965). At the end of the procedure, the bone defect was covered with the temporalis muscle and skin was closed with clamps ($n = 22$ animals). In sham-operated control

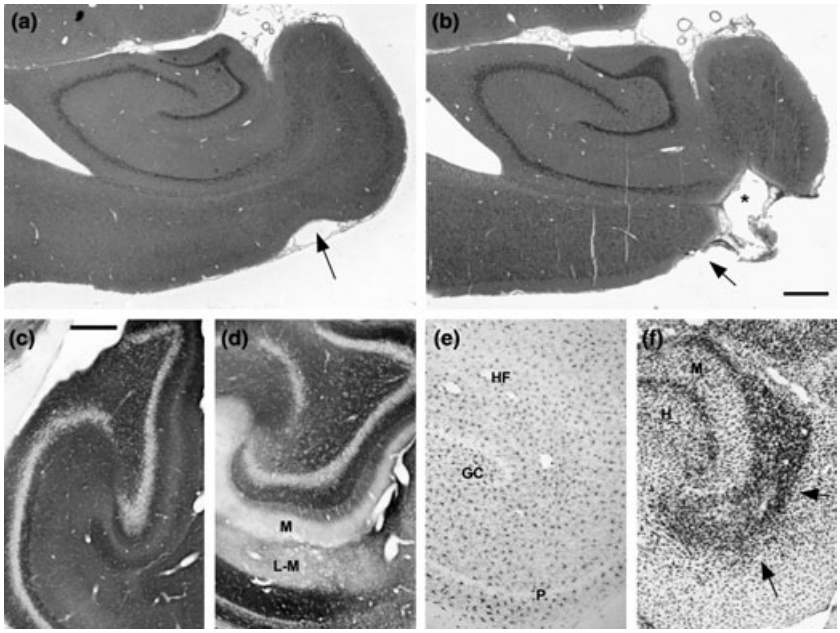

Fig. 1 Histological and immunohistochemical analysis of brains following lateral entorhinal cortex ablation (LECA). (a) and (b) show haematoxylin–eosin-stained horizontal sections of the temporal region of control (SOC, a) and lesioned (LECA, b) brains. Arrows indicate the rhinal sulcus (a, b). An asterix marks the position of the LECA (b), which penetrates through every layer of the entorhinal cortex. (c) and (d) illustrate synapsin I immunoreactivity in SOC (c) and LECA (d) animals. Note the marked reduction in the synapsin I synaptic marker immunoreactivity in the molecular layer (M) of the dentate gyrus (DG) and stratum lacunosum-moleculare (LM, d). (e) and (f) illustrate anti-rat CD11b stained microglia in SOC (e) and LECA (f) hippocampi. Arrows on (f) point to the deafferented layers with proliferating CD11b marker positive microglial cells. GC, granule cell layer of DG; HF, hippocampal fissure; H, hilum of the DG; M, molecular layer of the DG. Scale bars: 1 mm (a, b), 250 μm (c–f).

(SOC) animals the same procedure was performed except for coagulation – the meninges and the brain were not injured ($n = 21$ animals).

Immunohistochemical detection of synapsin I and CD11b

The first group of animals (two LECA and two SOC) was investigated 3 days after the surgery. The animals were anaesthetized with diethyl ether and perfused through the heart with 4% (w/v) paraformaldehyde in 0.1 M phosphate buffer (pH 7.4). The same transcardial perfusion fixation method was applied to other experimental rats unless otherwise indicated. The brains were kept in fixative overnight, then washed in phosphate-buffered saline (pH 7.4), cryoprotected in 25% (w/v) sucrose and 25-μm sections were prepared using a freezing microtome. Tissue sections were processed for the immunohistochemical detection of synapsin I (rabbit anti-synapsin I, 1:1000 dilution; Alexis Corporation, San Diego, CA, USA) and the microglia antigen CD11b specific mouse antibody (clone MRC OX-42, 1:100 dilution; Serotec, Oxford, UK), using the streptavidin–peroxidase method with 3′3′-diaminobenzidine tetrahydrochloride (DAB) substrate.

Electrophysiological analysis

The second group of animals (seven LECA and six SOC) recovered and survived for 10 days. Following Nembutal® anaesthesia (50 mg/kg, i.p.), the head was fixed in a stereotaxic frame, and stainless steel electrodes were implanted over the LEC (A 5.5, L 6.0), and deep bipolar electrodes inserted into the hippocampus (P 3.3, L 2.0, V 3.0; Paxinos and Watson 1998) at both sides. An additional screw electrode over the cerebellum served as reference. The electrode leads were attached to a miniature socket fixed to the skull with dental acrylic cement. After 40 days postoperative period, the animals were placed into plastic recording chambers and connected to the recording instrument through slip-ring assemblies. The instrument and the recording chamber were located in separate rooms. The behaviour of the animals was monitored with video cameras. Convulsions were induced with intraperitoneal injection of 5 mg/kg 4-AP. Spontaneous electroencephalography (EEG) signals were continuously recorded for 8 h following the 4-AP treatment. Signals were amplified 1000-fold with a multichannel amplifier (Elsoft Co., Budapest, Hungary), filtered (between 0.3 and 100 Hz), digitized and stored for off-line analyses using Digidata 1200B (Axon Instruments, CA, USA). Every seizure was characterized by a high-frequency spike train (tonic phase), and a following spike-and-wave period (clonic phase). The onset of tonic phase, which followed a wild running and/or jumping period, and the beginning of the clonic phase were assigned on the basis of the change of characteristic shape of waves and pattern of activity (Iida *et al*. 1998). The characteristic discharge frequencies were determined both in tonic and clonic phases (Figs 2a and b). The electrophysiological data were analysed by the Origin 7.5 software (OriginLab, Northampton, MA, USA), and the data were compared with the Neuman-Keuls test (post hoc test: ANOVA) at a minimum confidence level of $p < 0.05$.

Following EEG recording, the animals were anaesthetized with diethyl ether and perfused through the heart with fixative as

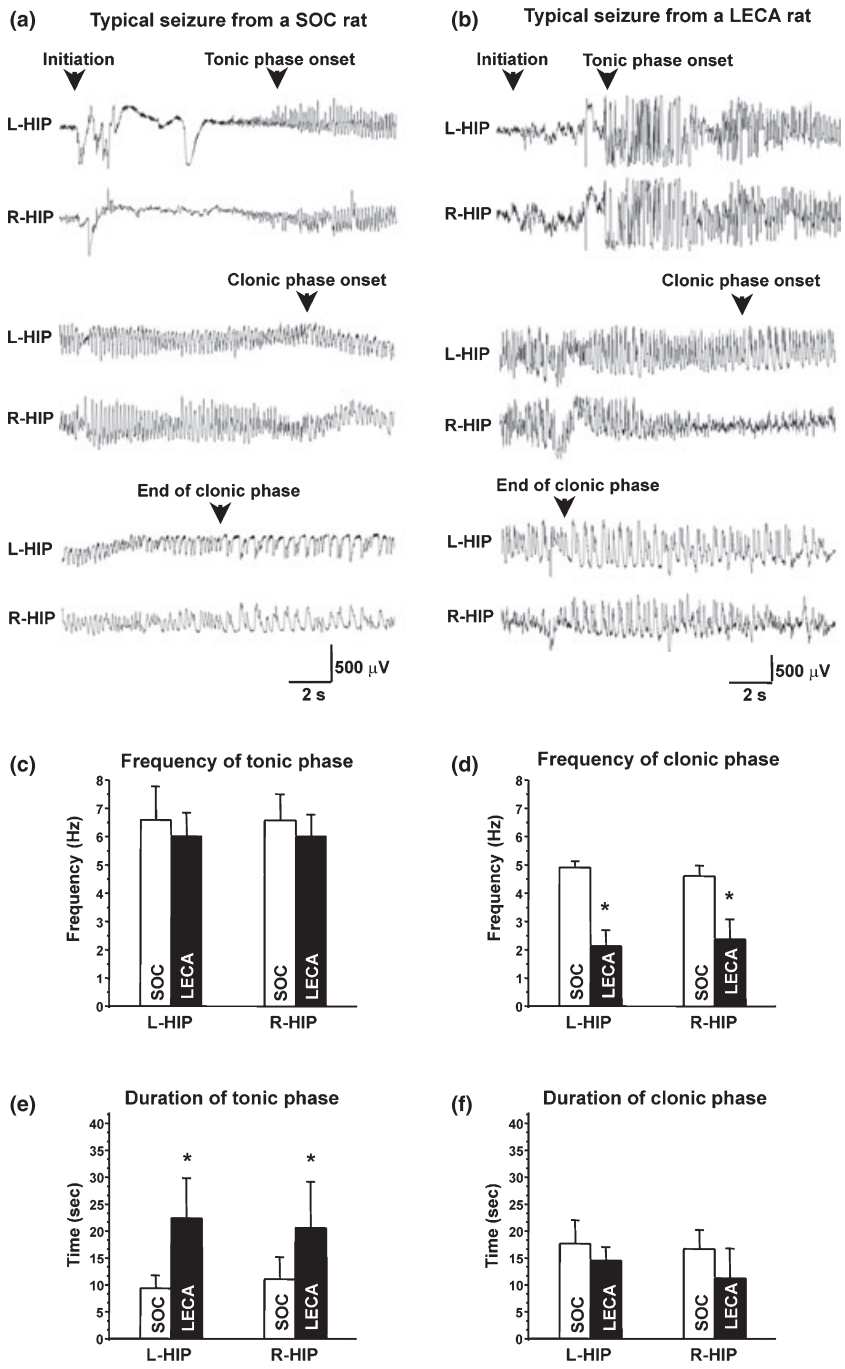

Fig. 2 Electroencephalography (EEG) traces and statistical differences between the tonic and clonic phases of hippocampal seizures in sham-operated control (SOC) and lateral entorhinal cortex ablation (LECA) animals. (a) and (b) show intrahippocampal EEG records of the tonic–clonic 4-aminopyridine (4-AP)-induced seizure in SOC (a) and LECA animals (b). The traces are representative sections of continuous records from single animals, displaying the first brief seizure episode following 4-AP injection. The onset of the seizure (initiation), the beginning of the tonic phase (top panel), the beginning and end of the clonic phase (middle and bottom panels, respectively) are indicated by arrows. (c–f) Pooled data from experiments carried out on seven LECA and six SOC animals illustrate the frequency and duration of the tonic and clonic EEG phases in the left- and right hippocampi of control (white columns) and operated (black columns) animals. SEM is indicated, asterisks show significant differences ($*p < 0.05$). Abbreviations: LECA, lateral entorhinal cortex ablation; SOC, sham-operated control; L-HIP, left hippocampus; R-HIP, right hippocampus.

described above. The precise location and extent of the surgery was assessed by histological analysis of LECA ($n = 3$) and SOC ($n = 3$) brains using haematoxylin–eosin-stained 5-μm paraffin embedded sections. The numbers of the neuronal cell bodies in CA1, CA2, CA3 and the hilum and granule cell layer of the dentate gyrus were counted and analysed as described below.

c-*fos* immunohistochemistry

The third group of animals (three LECA and three SOC rats) survived 40 days after the surgery. Three hours following the induction of convulsions by a single injection of 4-AP (5 mg/kg, i.p.), they were perfused through the heart with 4% (w/v) paraformaldehyde in 0.1 M phosphate buffer (pH 7.4). The brains were processed for c-*fos* immunohistochemistry as described previously (Mihály *et al.* 1997, 2001). Quantitative analysis was performed on five sections per animal. Areas of interest (AOI) for counts of neuronal nuclei were selected from regions CA1, CA2 and CA3 of the Ammon's horn, and from the granule cell layer and the hilum of the dentate gyrus. Within each AOI, the neuronal cell nuclei were counted using a Nikon Eclipse 600 microscope equipped with a SPOT RT Slider digital camera (1600 × 1200 dpi in 8 bits), using the Image Pro Plus 4.5 morphometry software

(Media Cybernetics, Silver Spring, MD, USA). In the regions of the Ammon's horn, and granule cell layer, cell counts were done using a 40 × objective. The AOIs were determined using the rectangular field of the camera including the pyramidal and granule cell layers. At the hilum of the dentate gyrus a 20 × objective was used to prepare the images, then the borders of the hilum (Amaral 1978) were outlined and counting was performed. The thickness of each section was measured with a 40 × DIC dry objective using Marzhauser MultiControl 2000 motorized stage mounted to microscope and Scope-Pro Plug-In Module for Image-Pro Plus 4.5. The real thickness was rectified for a refractive index (Glaser 1982) due to the dry objective used. Finally cell counts were normalized to 1 mm^3 of tissue, and analysed using *t*-test. The mean values of the cell numbers of the operated and contralateral sides were compared at a $p < 0.05$ significance level. Statistical analysis was done with the SPSS 9.0 computer program (SPSS Inc., Chicago, IL, USA).

Acetylcholinesterase staining and calretinin immunohistochemistry

The fourth group of animals (six LECA and six SOC rats) were killed 40 days after the surgery and their brains were processed for acetylcholinesterase (AChE) histochemistry (three–three animals) and calretinin immunohistochemistry (three–three animals). Following perfusion fixation, the brains were removed, and immersed in the fixative overnight at 4°C, then incubated in 30% (w/v) sucrose in 100 mM Tris-HCl; pH 7.8 (Tris buffer). Serial horizontal sections (25 μm) were cut using a freezing microtome. Sections were collected in Tris buffer containing 0.9% (w/v) NaCl (Tris-buffered saline) and kept at 4°C until use. Free-floating sections were pretreated in a solution containing 3% (v/v) H_2O_2 and 3% (v/v) Triton X-100 in Tris-buffered saline for 10 min. Then, sections were rinsed in Tris-buffered saline three times, and treated in 0.2 mM ethopropazine (Sigma, St Louis, MO, USA) in the dark for 30 min to inhibit the non-specific cholinesterase activity (Tago *et al*. 1986). Following three rinses in phosphate buffer, sections were incubated in 1:15 dilution of Karnovsky and Roots medium (Karnovsky and Roots 1964) in phosphate buffer for 30 min at room temperature. After washing in Tris buffer (three changes), sections were incubated in 0.05% (w/v) DAB and 0.005% (v/v) H_2O_2 in Tris buffer until detectable coloured reaction end-product appeared. Sections were mounted on glass slides, and covered with Entellan®. Calretinin immunohistochemistry was performed on horizontal free-floating sections, using the streptavidin–peroxidase method, DAB substrate and nickel-chloride intensification. Primary antibody (rabbit anti-calretinin; Zymed Laboratories Inc., South San Francisco, CA, USA) was used at 1:5000 dilutions. The optical density of AChE-positive nerve fibers was measured on digitalized images using the Image Pro Plus software. The number of calretinin-positive neurones was counted with the same software in the dentate gyrus (see the description of cell counting procedure above). The optical density of the calretinin-immunoreactive nerve fibers was measured in the molecular layer of the dentate gyrus and in strata oriens and radiatum of CA1. Statistical analysis was done with the SPSS 9.0 computer program (SPSS Inc.).

Histoblot analysis of ionotropic glutamate receptor proteins

The fifth group of rats (four LECA and four SOC) were killed 40 days after the surgery and used to determine changes in the distribution of AMPA, NMDA and kainate type iGluR subunit proteins, using an *in situ* blotting technique (histoblot, Tonnes *et al*. 1999; Gallyas *et al*. 2003). In brief, animals were deeply anaesthetized with diethyl ether, decapitated and the brains were quickly frozen in isopentane and stored at −80°C until sectioning. Horizontal cryostat sections (10 μm) were apposed to nitrocellulose membranes, which were previously moistened with 48 mM Tris-base, 39 mM glycine, 2% (w/v) sodium dodecyl sulfate and 20% (v/v) methanol for 15 min at room temperature. After blocking in 5% (w/v) non-fat dry milk in phosphate-buffered saline, nitrocellulose membranes were DNase I-treated (5 U/mL), washed and incubated in 2% (w/v) sodium dodecyl sulfate, 100 mM β-mercaptoethanol in 100 mM Tris-HCl (pH 7.0), for 60 min at 45°C to remove adhering tissue residues. After excessive washing, blots were reacted with affinity-purified anti-GluR1–4 (Pickard *et al*. 2000), anti-NR-1 (Molnar *et al*. 1995) and anti-KA-2 (Molnar *et al*. 1995) subunit specific antibodies (0.5 μg/mL) in blocking solution overnight, at 4°C. The bound primary antibodies were detected with alkaline phosphatase-conjugated anti-rabbit IgG secondary antibody (Tonnes *et al*. 1999). To facilitate the identification of structures and cell layers, adjacent cryostat sections were stained with cresyl violet. Digital images were acquired by scanning the membranes using a desktop scanner. Image analysis and processing were performed using the Adobe® Photoshop® software (Adobe Systems, San Jose, CA, USA). When processing the images, each was treated identically to allow comparison of pixel densities in different hippocampal regions. The pixel density of immunoreactivity was measured by an experimenter blind to the experimental conditions using a previously established quantification strategy (Xu *et al*. 2004). Briefly; open circular cursors with a diameter of 0.10 mm was placed at adjacent positions along the stratum oriens (8 circles), stratum radiatum (6 circles), stratum lacunosum-moleculare (7 circles), stratum moleculare of dentae gyrus (12 circles), hilum of dentate gyrus (6 circles) and stratum lucidum of CA3 (7 circles). The average of 10 background determinations (carried out near the brain protein-containing areas of the immunostained nitrocellulose papers) was subtracted from the average pixel densities measured within various hippocampal regions. Following background corrections, the average pixel density for the whole sub region of the hippocampus from one animal counted as one 'n'. Data were analysed and plotted using a GraphPad® Version 4.0. Differences between the corresponding hippocampal regions of LECA and SOC animals were assessed using a two-way analysis of variance (ANOVA), and further compared with the Bonferroni *post hoc* test, at a minimum confidence level of $p < 0.05$.

Results

Characterization of animals after lateral entorhinal cortex ablation

Animals were subjected to regular observation following surgery. During daytime examinations (2–4 h per day), we did not encounter spontaneous seizure symptoms following LECA. Histological analysis of the lesion on thin paraffin sections 40 days after surgery confirmed the complete removal of the LEC (Fig. 1b). In addition to whole layers of the LEC,

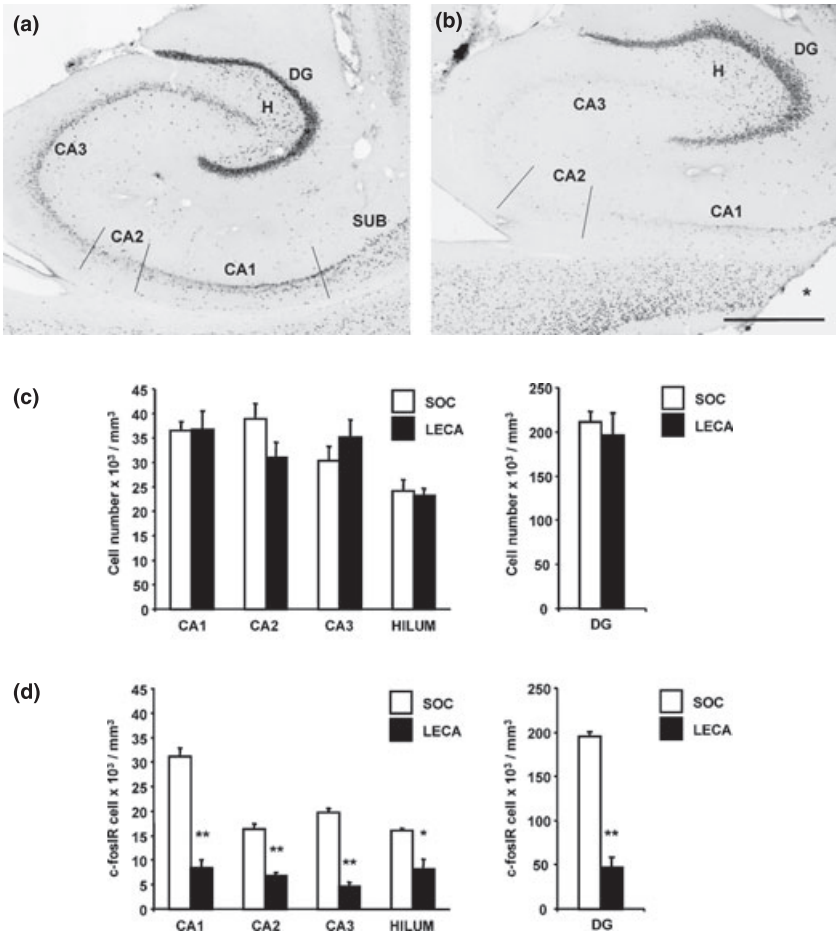

Fig. 3 Assessment of the number of neurones and differences in the appearance of c-*fos* immunoreactivity in control and lateral entorhinal cortex ablation (LECA) animals following 4-aminopyridine (4-AP)-induced seizures. c-*fos* immunoreactivity in the left hippocampi of sham-operated control (SOC) (a) and LECA animals (b). Abbreviations: DG, dentate gyrus; H, hilum of DG; CA1, CA2, CA3, hippocampal subfields; SUB, subiculum. Asterisk indicates the site of the lesion. Scale bar: 500 μm. (c) the number of nerve cell bodies does not change in LECA animals compared with controls: the cell counts from the left hippocampi were obtained from haematoxylin–eosin-stained horizontal sections (5 μm) 40 days after the surgery. (d) On the side of the lesion, the number of c-*fos* immunopositive cell nuclei decreases significantly in LECA animals, compared with controls (cell counts from left hippocampi). Asterisks indicate significant differences, $^{*}p < 0.002$, $^{**}p < 0.001$.

the lesion regularly affected the subcortical white matter (Fig. 1b). There was no noticeable neuronal loss in the hippocampal region at the side of the LECA (Figs 1a, b and 3c). Immunohistochemical analysis performed 3 days postlesion revealed the disappearance of synapsin I immunoreactivity (Figs 1c and d), and microglia proliferation (Figs 1e and f) in the outer molecular layer of the dentate gyrus and in stratum lacunosum-moleculare of hippocampal regions CA1–3. Microglia proliferation was also noticeable in stratum oriens of the regio superior in the termination zone of the temporoammonic path (not shown). These changes confirmed the ongoing degeneration of the perforant- and temporoammonic path axons on the side of the lesion, 3 days following surgery.

Electrophysiological analysis of 4-aminopyridine-induced seizure susceptibility in animals with and without lateral entorhinal cortex ablation

Following 4-AP injection (5 mg/kg i.p.) generalized tonic–clonic seizures developed in every control (SOC) animal. In all SOC animals, at least two seizures were detected during the 8-h recording period (2.6 seizures per animal). By contrast, in the LECA group ($n = 7$) only three animals responded to 4-AP injection with a single seizure and the remaining four animals produced no seizure at all. In the SOC group the first seizure lasted for 55.5 ± 4.2 s, and developed during the first 30 min following the 4-AP injection with an average latency of 20.8 ± 6.4 min. These events were followed by a second seizure within the first hour following the 4-AP treatment. The mean delay between the two seizures was 16.2 ± 4.9 min. The second seizure was longer, lasted for 73.4 ± 13.9 s. In the LECA group the latency of first seizure increased to 31.8 ± 4.3 min, and only one rat presented a second epileptic event.

There were differences between the EEG activities of SOC and LECA animals (Figs 2a and b).

During the tonic phase the frequency did not change significantly (Fig. 2c, L-HIP/SOC: 6.6 ± 1.2 Hz; L-HIP/LECA: 6.0 ± 0.8 Hz; R-HIP/SOC: 6.6 ± 0.9 Hz; R-HIP/LECA: 6.0 ± 0.8 Hz; $n = 6$ SOC, $n = 7$ LECA), but this phase of the convulsion was significantly longer in LECA animals; ∼240% increase in the left hippocampus and ∼187% increase in the right hippocampus (Fig. 2e, L-HIP/SOC: 9.3 ± 2.4 s; L-HIP/LECA: 22.4 ± 7.5 s; R-HIP/SOC: 11.0 ± 4.2 s; R-HIP/LECA: 20.6 ± 8.5 s; $p < 0.05$). A slight increase of the spike amplitudes was detected; however, this difference was not significant.

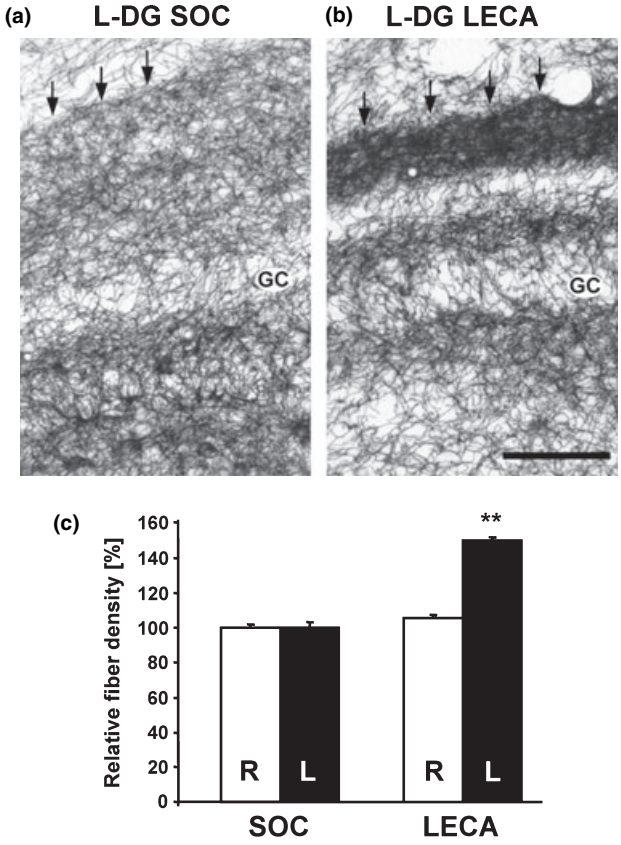

Fig. 4 Identification of sprouting of acetylcholinesterase (AChE) positive nerve fibers in the hippocampus following lateral entorhinal cortex lesion. AChE-containing nerve fibers in the left dentate gyrus (L-DG) of sham-operated control (SOC) (a) and lateral entorhinal cortex ablation (LECA) (b) animals. Arrows point to the hippocampal fissure. Note the shrinkage of the dentate molecular layer in (b). GC, granule cell layer of the dentate gyrus. In LECA animals (b), the outer molecular layer displays strong AChE staining (arrows). Stronger staining is also apparent at the inner molecular layer (just above the GC). Scale bar: 100 μm. (c) Densitometry of the molecular layer of the dentate gyrus indicates a significant (**$p < 0.001$) increase in AChE-positive fibre density on the side of the LECA (black columns, L) compared with the corresponding contralateral region (white columns, R).

As to the clonic phase, the frequency decreased significantly in LECA animals (~43% decrease in left hippocampus, and ~30% decrease in the right hippocampus (Fig. 2d, L-HIP/SOC: 4.9 ± 0.2 Hz; L-HIP/LECA: 2.1 ± 0.6 Hz; R-HIP/SOC: 4.6 ± 0.4 Hz; R-HIP/LECA: 2.3 ± 0.7 Hz; $p < 0.05$), without detectable changes in the duration of this phase (Fig. 2f, L-HIP/SOC: 17.7 ± 4.4 s; L-HIP/LECA: 14.5 ± 2.5 s; R-HIP/SOC: 16.7 ± 3.5 s; R-HIP/LECA: 11.2 ± 5.6 s).

In summary, the EEG analysis of freely moving animals indicated that the lateral entorhinal lesion decreased the number of hippocampal brief convulsions, and increased the latency of the seizure. At the same time, those animals that displayed seizure, presented a significantly longer tonic phase, and thereby a longer seizure event.

Identification of changes in c-*fos* expression following 4-aminopyridine-induced seizures

To verify the EEG alterations indicating decreased 4-AP-induced seizure susceptibility, we used the immunohistochemical analysis of c-*fos* expression in rat brains with and without LEC lesion to obtain information about the extent of neuronal populations activated during seizures. Previous studies established that c-*fos* is a reliable indicator of neuronal activity in 4-AP-induced seizures (Mihály *et al*. 2001, 2005; Szakács *et al*. 2003). Convulsions induced by 4-AP 40 days after the surgery caused the expression of c-*fos* protein in every part of the hippocampus and the subiculum (Figs 3a and b). The overall pattern of c-*fos* immunoreactivity (c-*fos*IR) in SOC and LECA animals 3 h after the 4-AP injection was similar to our previous findings obtained with intact animals (Mihály *et al*. 2001, 2005; Szakács *et al*. 2003): strong c-*fos*IR in the dentate granule cell layer, medium c-*fos*IR in the stratum pyramidale of CA1–3, and scattered c-*fos*IR nuclei in the hilum of the dentate gyrus, and in the infra- and suprapyramidal layers of CA1–3 (Figs 3a and b). Quantitative analysis of immunostained cell nuclei revealed that the convulsions in LECA animals induced significantly less c-*fos* immunopositive cells in the pyramidal cell layer of the Ammon's horn, and in the granule cell layer and in the hilum of the dentate gyrus, compared with the SOC group (Fig. 3d). Because the number of the haematoxylin–eosin-stained cell bodies did not change in LECA brains (Fig. 3c), the significant reduction in the number of c-*fos* immunopositive cells (Fig. 3d) indicates the decrease of neuronal activity, and not the loss of neurones in the investigated hippocampal regions.

Identification of sprouting in the hippocampus following lateral entorhinal cortex lesions

To investigate the rewiring pattern of afferents following LECA, we analysed changes of the cholinergic innervation (Nadler *et al*. 1977), and the relative density of calretinin-positive nerve fibers (Deller and Frotscher 1997). AChE-positive nerve fibers were detected in every part of the hippocampus. On the side of the LECA, the density of the AChE-positive structures increased significantly only in the outer molecular layer of the dentate gyrus, where a dense band of cholinergic axons occupied the place of the degenerated perforant path terminals (Figs 4a and b). Another dense band of AChE staining was seen in the inner molecular layer, just above the granule cells (Fig. 4b).

Calretinin-positive cell number in the dentate gyrus decreased significantly in the LECA animals, compared with the SOC group (Figs 5a–d). The decrease was significant not only on the operated side, but also in the contralateral hippocampus of the LECA animals (Fig. 5e). Sprouting of

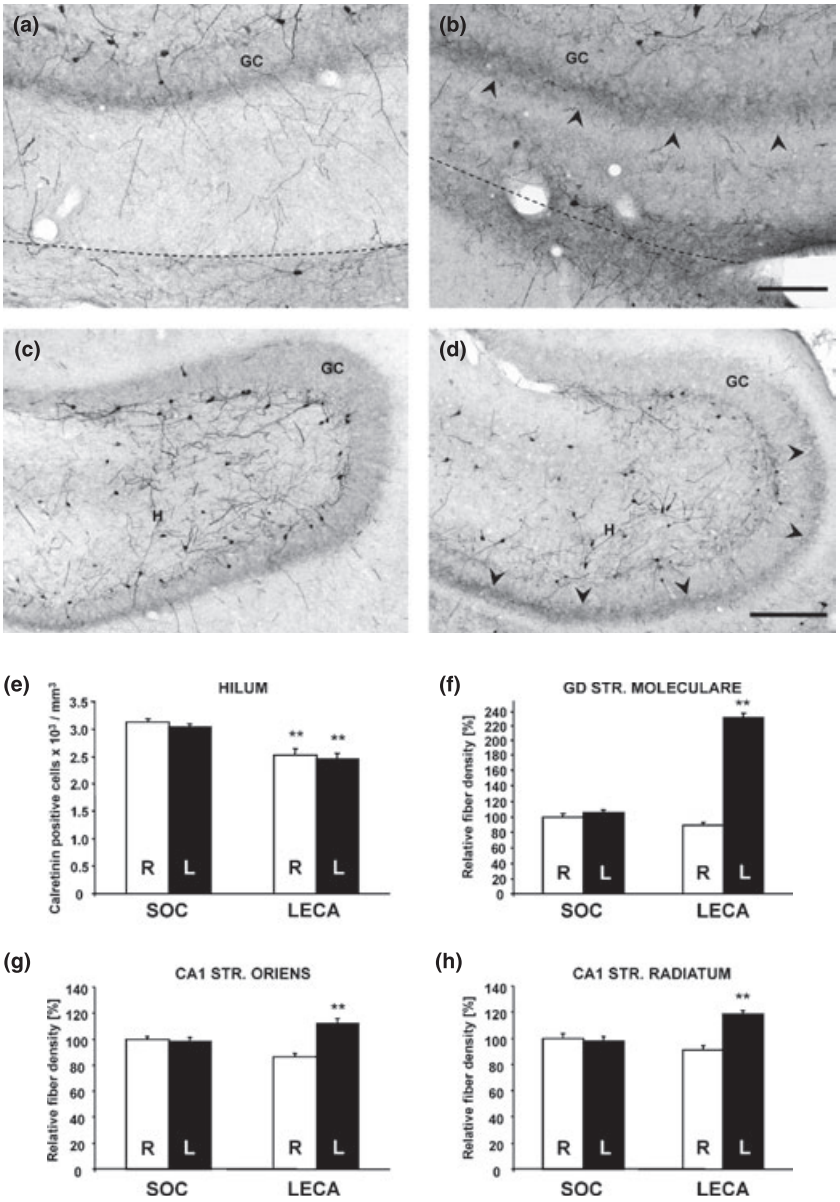

Fig. 5 Calretinin immunohistochemistry of sham-operated control (SOC) (a, c) and lateral entorhinal cortex ablation (LECA) (b, d) left hippocampi (H, hilum of the dentate gyrus; GD, dentate gyrus; GC, granule cell layer; arrows indicate the hippocampal fissure; bar: 100 μm). Note the shrinkage of the molecular layer (the broken line represents the hippocampal fissure), and the thick, immunostained zone in the inner molecular layer, indicating calretinin positive fibre sprouting (arrowheads). Scale bars: 100 μm (a, b); 250 μm (c, d). (e) The number of calretinin immunopositive neurones decreased significantly in LECA animals in both hippocampi (**$p < 0.001$). (f) The relative calretinin fibre density in the whole thickness of the molecular layer increased significantly on the side of LECA (**$p < 0.001$). (g and h) The calretinin-positive fibre density is significantly increased in the strata oriens and radiatum of the CA1 region (**$p < 0.001$).

the calretinin-positive fibers was also noticeable. In the inner molecular layer of the dentate gyrus new fibers were found, which penetrated the middle segment of the molecular layer (Figs 5b and f). The density of calretinin-positive nerve fibers increased not only in the dentate gyrus, but also in the regio superior. The stratum oriens and the stratum radiatum displayed significant increase, indicating the sprouting of calretinin-positive elements in these layers (Figs 5g and h).

Characterization of region specific changes in the expression of ionotropic glutamate receptor proteins following lateral entorhinal cortex lesions

To identify region specific differences in the expression pattern of iGluRs, adjacent horizontal sections of whole unfixed SOC and LECA brains were blotted onto nitrocellulose membranes prior to immunostaining as described previously (Tonnes *et al*. 1999; Gallyas *et al*. 2003). This 'histoblot' method is a reliable and convenient way to compare the regional distribution and expression pattern of different receptor proteins in the brain. The AMPA receptor subunits GluR1–4 were localized in strata oriens, radiatum and lacunosum-moleculare of CA1–3, and in the molecular layer of the dentate gyrus (Fig. 6a, GluR1–4). The $GluR1_{flop}$ splice variant specific antibody (Tonnes *et al*. 1999) produced strong immunolabelling in the strata radiatum and oriens of CA1 and in the dentate molecular layer, whereas much weaker reactivity was seen in the CA1 stratum pyramidale and in the dentate granule cell layer (Fig. 6a, $GluR1_{flop}$). The CA3 region showed a very weak labelling with the anti-$GluR1_{flop}$ antibody. The NR1 and

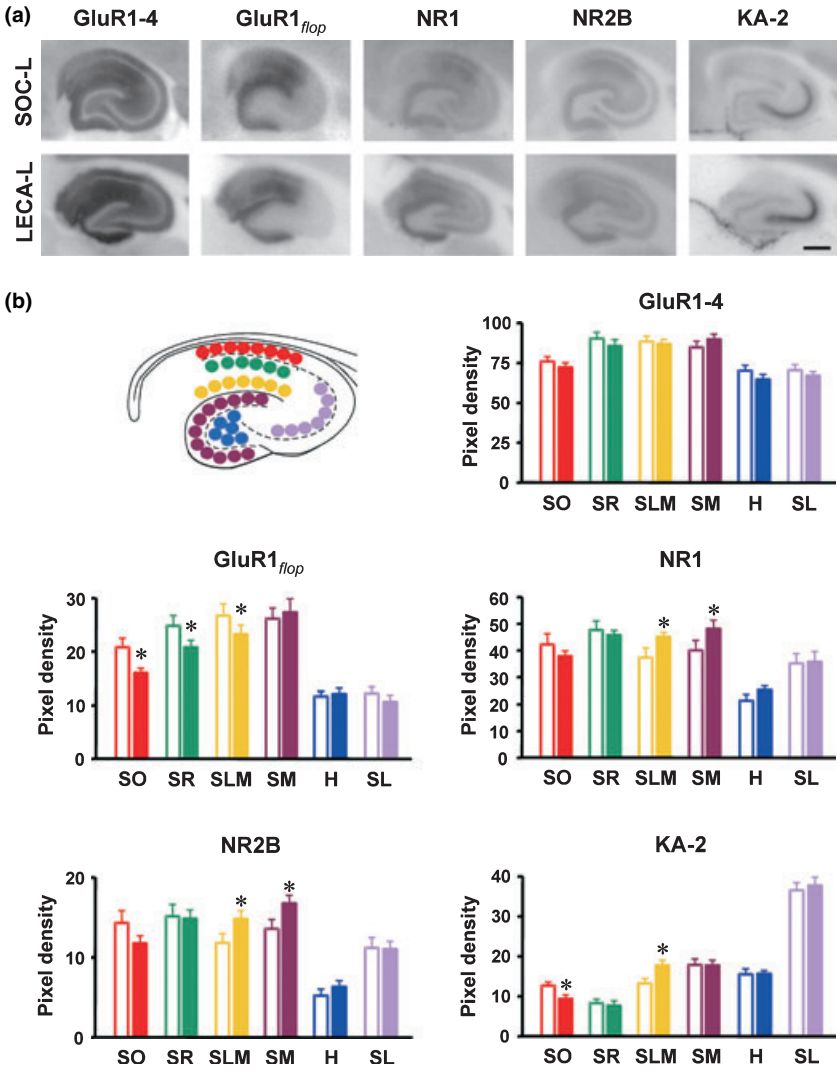

Fig. 6 Effect of lateral entorhinal cortex ablation (LECA) on the distribution and density of ionotropic glutamate receptor subunits in the hippocampal formation. (a) Representative histoblots of corresponding left hippocampal regions of sham-operated control (SOC) and LECA animals immunostained with the indicated antibody against GluR1–4, GluR1$_{flop}$, NR1, NR2B and KA-2 ionotropic glutamate receptor (iGluR) subunits. Scale bar: 1 mm. (b) Schematic diagram illustrate the sampling method used to compare immunoreactivities in different hippocampal regions (see methods for details). The colours represent layers of the hippocampal formation: red, stratum oriens (SO); green, stratum radiatum (SR); yellow, stratum lacunosum-moleculare (SLM); plum, stratum moleculare of dentate gyrus (SM); blue, hilum of dentate gyrus (H); lilac, stratum lucidum of CA3 (SL). Density readings were taken by placing open circular cursors with a diameter of 0.1 mm at the indicated adjacent positions along SO (8), SR (6), SLM (7), SM (12), H (6), SL (7). The bar diagrams indicate the pixel density levels (arbitrary units) in various hippocampal regions in SOC and LECA animals for the indicated iGluR subunit. Asterisk indicates significant differences (*$p < 0.05$).

NR2B NMDA receptor subunit immunoreactivities displayed a similar, overlapping distribution pattern in the strata oriens and radiatum of CA1, and in the outer molecular layer of the dentate gyrus (Fig. 6a, NR1 and NR2B). The KA-2 kainate receptor subunit was localized mainly in the stratum lucidum of CA3, and in the inner molecular layer (just above the granule cell layer) of the dentate gyrus (Fig. 6a, KA-2).

Densitometry analysis was carried out to compare the immunoreactivity in the corresponding hippocampal regions of SOC and LECA animals. Although there were no detectable changes in the density of total AMPA receptor subunit staining (Fig. 6b, GluR1–4), the GluR1$_{flop}$ splice variant displayed a significant decrease ($p < 0.05$) in every layer of the CA1 region: strata oriens (23.2 ± 4.1%), radiatum (16.2 ± 5.2%) and lacunosum-moleculare (13.1 ± 6.2%) in LECA animals (Fig. 6b, GluR1$_{flop}$). The labelling density of both NR1 and NR2B NMDA receptor subunits displayed a very similar increase in the deafferented layers (molecular layer of the dentate gyrus NR1: 20.3 ± 8.0%; NR2B: 23.5 ± 7.2%; stratum lacunosum-moleculare of CA1 NR1: 21.1 ± 4.1%; NR2B: 25.5 ± 8.6%) on the side of the LECA (Fig. 6b, NR1 and NR2B). The density of KA-2 subunit did not change in CA3, but displayed an increase in stratum lacunosum-moleculare of CA1 (34.3 ± 9.2%) and a decrease in stratum oriens (25.7 ± 6.8%) of the same hippocampal region (Fig. 6b, KA-2).

Discussion

Our correlated morphological, functional and molecular studies indicate that cholinergic and commissural sprouting and the rearrangement of iGluR subunits coincide with a marked decrease in hippocampal seizure susceptibility following LEC lesions. This underlines the importance of LEC in hippocampal seizure control, and the strong impact of the lateral perforant path and the temporoammonic pathway on the synaptic organization of the hippocampus.

Chronic lateral entorhinal cortex lesion leads to sprouting of cholinergic and commissural, calretinin-containing axons in the deafferented hippocampal areas

The perforant path originates from layer II/III pyramidal cells of the lateral and medial EC (Witter *et al*. 2000). Our paraffin-embedded sections confirmed that the surgical lesion penetrated not only the layers of the LEC, but also the subcortical white matter, destroying perforant path neurones together with axons of the temporoammonic tract. The lesions were confirmed by the presence of microglia proliferation in the stratum oriens and lacunosum-moleculare of the regio superior and in the outer molecular layer of the dentate gyrus. The degeneration of the perforant path was further indicated by the disappearance of synapsin I immunoreactivity in the early phase of the lesion. In the dentate molecular layer, a complete dropout of synapsin I immunoreactivity was observed only in the outer one-third, indicating that fibers originating from the MEC were not destroyed. These results are consistent with previous observations on the early neuropathological consequences of EC lesions (Deller and Frotscher 1997; Rappert *et al*. 2004). With conventional haematoxylin–eosin staining, there was no detectable neuronal cell loss in the hippocampus 40 days after the LECA.

EC lesions are themselves epileptogenic (Deller and Frotscher 1997; Schwarz *et al*. 2000). Destruction of the EC and the degeneration of the perforant path release glutamate in target synaptic regions. This glutamate release and the denervation supersensitivity cause the transient limbic seizures in experimental animals (Deller and Frotscher 1997). However, these are early symptoms, and after 40 days of recovery, the empty synaptic sites are already innervated by collateral sprouting from other fibre systems (Deller and Frotscher 1997). The role of these sprouting axons in the modulation of seizure activity following chronic EC lesions is not clear (Bragin *et al*. 1997).

Chronic lateral entorhinal cortex lesion reduces the seizure susceptibility of the hippocampus

The latency of the appearance of the first convulsion was longer in our LECA animals compared with controls. The number of spontaneous seizure events decreased in the LECA animals, indicating the increase of the threshold of convulsion in deafferented hippocampi. Comparison of the tonic and clonic phases showed that the frequency of EEG discharges in the clonic phase decreased, whereas the duration of the tonic phase increased. These EEG changes suggest that the LEC plays an important role in the initiation of hippocampal seizures, probably through the perforant pathway and the reciprocal connections between the MEC and LEC (Mitchell and Ranck 1980; Iijima *et al*. 1996; Dolorfo and Amaral 1998). The ability of the EC to generate epileptiform activity has been described previously in brain slice models (Stringer and Lothman 1992; Weissinger *et al*. 2000) and *in vivo* (Scharfman 1996). Combined EC–hippocampal slices indicated that the origin of epileptiform discharges was in the EC, which spread to the dentate gyrus and the CA3 pyramidal cells (Stoop and Pralong 2000; D'Antuono *et al*. 2001). In our experiments the number of the seizures decreased but the tonic phases (and the whole seizure) were significantly longer, which is consistent with the proposed weakening of GABA-ergic inhibition due to the loss of feed-forward drive from the EC (Acsády *et al*. 1998). The loss of feed-forward inhibition can be explained partly with the absence of the lateral perforant path (innervating the stratum lacunosum-moleculare) and partly with the degeneration of the temporoammonic pathway, which normally originates from the MEC and innervates the dendrites of basket cells in the stratum oriens of the regio superior (Raisman *et al*. 1965). The most probable consequence of the loss of the temporoammonic pathway is the weakening or loss of feed-forward inhibition in stratum pyramidale of CA1 (Acsády *et al*. 1998; Barbarosie *et al*. 2000). This phenomenon could be the explanation of the long tonic phase in our experiments. The decrease of the number of seizure events was explained with the loss of the LEC and the consequent partial blockade of the spread of the neocortical seizure to the EC.

The removal of the EC in an *in vitro* experiment stops the reverberatory circuits and weakens, but does not abolish the hippocampal seizures (Stoop and Pralong 2000), because the hippocampus has its own CA3-dentate seizure generator: the CA3 region has several axon collaterals that provide excitatory feedback to the dentate gyrus (Li *et al*. 1994). Other important connections of the CA3 are to CA1, which also projects back to the MEC through the subiculum, so the MEC could well be responsible for the maintenance and re-initiation of the hippocampal seizure activity through the medial perforant path in our experiments. However, the lesion of the LEC disconnects the hippocampus from perirhinal cortices and therefore the impact of the neocortical convulsion on the MEC–hippocampal circuits weakens (Burwell and Amaral 1998). Recent *in vitro* experiments proved that the perirhinal cortex has its own seizure generator, which connects to the LEC (de Guzman *et al*. 2004). The LEC and MEC are interconnected and their interactions play important role in the reverberation and spread of convulsive activity to the hippocampus (Iijima *et al*. 1996; de Guzman *et al*. 2004). Ablation of the LEC disrupted the intraentorhinal reverberation, and also disconnected the EC from other, mainly neocortical inputs (Burwell and Amaral 1998). The consequence was the decrease of the number of hippocampal brief seizures detected in our experiments. Our results are supported by these *in vitro* experiments (Avoli *et al*. 2002; de Guzman *et al*. 2004).

The decrease of *c-fos* expression in LECA animals can be explained by the decrease of the number of brief seizures. Our recent experiments with 4-AP proved that *c-fos* mRNA expression is boosted regularly by the second and third brief convulsion (Mihály *et al*. 2005). Following LECA, animals

had only one brief hippocampal convulsion, despite the fact that the convulsive agent (4-AP) affected the hippocampus through the circulation. Furthermore, it is likely that the rearrangement of iGluR subunits, and the degeneration of a strong excitatory tract, also contribute to the protective effect (see below).

Chronic lateral entorhinal cortex lesion alters the level of expression and molecular organization of ionotropic glutamate receptors in the deafferented layers of the hippocampal formation

Lesioning of the EC protects hippocampal CA1 and CA3 neurones from ischemia- or stress-induced damage, and the interruption of the perforant path significantly decreases over-excitation of the dentate granule cells by glutamate (Jorgensen *et al*. 1987; Sunanda *et al*. 1997). Both NMDA and AMPA receptors play important roles in mediating overexcitation, because specific antagonists of both types of receptors effectively prevent the epileptiform activity (Bear *et al*. 1996). Deafferentation of the hippocampal formation, however, does not stop the epileptiform events, but prevents the development of sustained, recurrent seizure activity (White and Price 1993).

In this study we have identified region and subtype/subunit specific changes in the expression of iGluR proteins. Although the total amount of AMPA receptor subunits remained unchanged, GluR1$_{flop}$ displayed a significant decrease in the CA1 region. Previous autoradiography studies (Ułas *et al*. 1990b) are consistent with our results obtained with the GluR1–4 antibody, which reacts with all AMPA receptor subunit proteins (Pickard *et al*. 2000). This study reported a small, transient decrease in [^{3}H]AMPA binding in the molecular layer 3 days following unilateral lesions of the EC, which returned to control levels between 7 and 30 days postlesion followed by a moderate increase at day 60 (Ułas *et al*. 1990b). An immunocytochemical study of GluR1 and GluR2/3 AMPA receptor subunits identified no change between days 1–14 following lesioning of the perforant path (Mizukami *et al*. 1997). By contrast, 30–90 days postlesion, GluR1 immunolabelling was increased in the outer molecular layer of the dentate gyrus ipsilateral to lesion. The GluR2/3 immunolabelling was also increased moderately within the same region, although the intensity of the staining was less than that observed for GluR1 (Mizukami *et al*. 1997). The reported increase in total GluR1 immunostaining (Mizukami *et al*. 1997) may be due to the selective up-regulation of the developmentally earlier GluR1$_{flip}$ splice variant in the deafferented regions of the hippocampus. The decrease of GluR1$_{flop}$ level in our experiments may reflect changes of activity-dependent recruitment of GluR1 subunits to the deafferented postsynaptic sites (Molnar *et al*. 2002). It is generally accepted that the recruitment of GluR1-containing AMPA receptors to the synapse is an activity-dependent process, whereas GluR2 subunits appear to be inserted in a constitutive and activity-independent manner (reviewed in Molnar and Isaac 2002). This may explain the more robust changes in GluR1 compared with other AMPA receptor subunits in the deafferented layers of the hippocampus.

At 30–60 days after unilateral entorhinal lesion an increase in NMDA-displaceable [^{3}H]glutamate binding in the dentate gyrus was reported (Ułas *et al*. 1990b; Nicolle *et al*. 1997). Our study suggested that the increased NMDA receptor binding activity was due to the increased expression of both NR1 and NR2B subunit proteins. Previous quantitative *in situ* hybridization mRNA expression analysis and immunohistochemical comparisons also identified an increase in NR1 at 5–9 days following unilateral transection of the perforant path (Gazzaley *et al*. 1997; Iwakiri *et al*. 2002), which is consistent with our findings.

Previous studies reported an elevation of the [^{3}H]kainate binding 21–30 days postlesion (Ułas *et al*. 1990a; Nicolle *et al*. 1997) in areas where we identified increased KA-2 immunoreactivity. The decrease of KA-2 immunoreactivity in CA1 stratum oriens could well be the consequence of the degeneration of the temporoammonic pathway and the consecutive decrease of glutamatergic input. The increase of KA-2 in stratum lacunosum-moleculare may reflect activity changes in the terminals from the medial perforant path.

Following the lesion of the lateral perforant pathway, shrinkage of the molecular layer of the dentate gyrus develops (Caceres and Steward 1983). Therefore we have to consider that our observations of an increase in NMDA and kainate receptor immunoreactivity may simply reflect an increase in the density of receptor proteins due to reduction in tissue volume. However, the fact that in adjacent sections the GluR1$_{flop}$ and GluR1–4 AMPA receptor subunit immunolabelling demonstrated a decrease, or no change, respectively, argues against the notion that the observed changes are due to tissue shrinkage. Therefore it is reasonable to conclude that the subunit-specific changes in iGluRs reflect postlesion reorganization of inputs within the deafferented layers of the hippocampus and may be relevant to functional recovery of the damaged circuits.

Conclusions

Our *in vivo* study of chronic LEC-lesioned rats proved the inhibition of the spread of the seizure from the neocortex to the hippocampus. The latency of the hippocampal seizure increased, and the number of brief convulsions decreased, indicating that the LEC is an important relay station between the neocortex and the hippocampus during the spread of neuronal hyperactivity. The chronic lesion of the LEC caused the overall decrease of seizure-related c-*fos* expression in the hippocampus, which proved the importance of repeated seizure episodes in the induction of neuronal c-*fos*

expression. However, the chronic lesion of the LEC did not abolish hippocampal seizure and related c-*fos* expression, indicating the pathophysiological significance of intrinsic hippocampal neuronal circuits and the MEC, which was preserved in our experiments. The chronic lesion also induced a pronounced sprouting of cholinergic axons and calretinin-containing fibres. The sprouting was accompanied by a down-regulation of GluR1$_{flop}$ splice variant without significant changes in the total amount of AMPA receptors in the deafferented zone of the hippocampus. We have also identified an increase in NR1/NR2B NMDA receptor and KA-2 kainate receptor subunits in the deafferented regions. These results suggest different response patterns for individual iGluR types and subunits to deafferentation and sprouting, and provide additional information about the role of the LEC. The LEC plays important role not only in the spread and regulation of hippocampal convulsive activity, but also in the maintenance and regulation of iGluR subunit content of postsynaptic membranes in the hippocampal target areas.

Acknowledgements

The experiments were supported by the Hungarian National Research Fund (OTKA T 32566), the British Council (GB-8/2003), MRC and the Wellcome Trust. The technical assistance of Mrs A. Imre-Kobolák, Mrs K. Lakatos, Mrs M. Herczegh-Kara and Mr S. M. Ball is appreciated. The monoclonal antibody to GluR1$_{flop}$ was provided by Professor Peter Streit (University of Zurich).

References

Acsády L., Kamondi A., Sík A., Freund T. and Buzsáki G. (1998) GABAergic cells are the major postsynaptic targets of mossy fibers in the rat hippocampus. *J. Neurosci.* **18**, 3386–3403.

Adams M. M., Gazzaley A. H. and Morrison J. H. (2001) Attenuated lesion-induced *N*-methyl-D-aspartate receptor (NMDA) plasticity in the dentate gyrus of aged rats following perforant path lesions. *Exp. Neurol.* **172**, 244–249.

Amaral D. G. (1978) A Golgi study of cell types in the hilar region of the hippocampus in the rat. *J. Comp. Neurol.* **182**, 851–914.

Avoli M., D'Antuono M., Louvel J., Kohling R., Biagini G., Pumain R., D'Arcangelo G. and Tancredi V. (2002) Network and pharmacological mechanisms leading to epileptiform synchronization in the limbic system *in vitro*. *Prog. Neurobiol.* **68**, 167–207.

Barbarosie M., Louvel J., Kurcewicz I. and Avoli M. (2000) CA3-released entorhinal seizures disclose dentate gyrus epileptogenicity and unmask a temporoammonic pathway. *J. Neurophysiol.* **83**, 1115–1124.

Bartolomei F., Khalil M., Wendling F., Sontheimer A., Regis J., Ranjeva J. P., Guye M. and Chauvel P. (2005) Entorhinal cortex involvement in human mesial temporal lobe epilepsy: an electrophysiologic and volumetric study. *Epilepsia* **46**, 677–687.

Bear J., Fountain N. B. and Lothman E. W. (1996) Responses of the superficial entorhinal cortex *in vitro* in slices from naive and chronically epileptic rats. *J. Neurophysiol.* **76**, 2928–2940.

Bragin A., Csicsvari J., Penttonen B. and Buzsaki G. (1997) Epileptic afterdischarge in the hippocampal–entorhinal system: current source density and unit studies. *Neuroscience* **76**, 1187–1203.

Burwell R. D. and Amaral D. G. (1998) Cortical afferents of the perirhinal, postrhinal and entorhinal cortices of the rat. *J. Comp. Neurol.* **398**, 179–205.

Caceres A. and Steward O. (1983) Dendritic reorganization in the denervated dentate gyrus of the rat following entorhinal cortical lesions: a Golgi and electron microscopic analysis. *J. Comp. Neurol.* **214**, 387–403.

D'Antuono M., Benini R., Biagini G., D'Arcangelo G., Barbarosie M., Tancredi V. and Avoli M. (2001) Limbic network interactions leading to hyperexcitability in a model of temporal lobe epilepsy. *J. Neurophysiol.* **87**, 634–639.

Del Turco D., Woods A. G., Gebhardt C., Phinney A. L., Jucker M., Frotscher M. and Deller T. (2003) Comparison of commissural sprouting in the mouse and rat fascia dentata after entorhinal cortex lesion. *Hippocampus* **13**, 685–699.

Deller T. and Frotscher M. (1997) Lesion-induced plasticity of central neurons: sprouting of single fibres in the rat hippocampus after unilateral entorhinal cortex lesion. *Prog. Neurobiol.* **53**, 687–727.

Dolorfo C. L. and Amaral D. G. (1998) Entorhinal cortex of the rat: organization of intrinsic connections. *J. Comp. Neurol.* **398**, 49–82.

Freund T. F. and Buzsaki G. (1996) Interneurons of the hippocampus. *Hippocampus.* **6**, 347–470.

Gallyas F. Jr, Ball S. M. and Molnar E. (2003) Assembly and cell surface expression of KA-2 subunit-containing kainite receptors. *J. Neurochem.* **86**, 1414–1427.

Gazzaley A. H., Benson D. L., Huntley G. W. and Morrison J. H. (1997) Differential subcellular regulation of NMDAR1 protein and mRNA in dendrites of dentate gyrus granule cells following perforant path transaction. *J. Neurosci.* **17**, 2006–2017.

Glaser E. M. (1982) Snell's law: the bane of computer microscopists. *J. Neurosci. Meth.* **5**, 201–202.

de Guzman P., D'Antonuo M. and Avoli M. (2004) Initiation of electrographic seizures by neuronal networks in entorhinal and perihinal cortices in vitro. *Neuroscience* **123**, 875–886.

Hjorth-Simonsen A. and Jeune B. (1972) Origin and termination of the hippocampal perforant path in the rat studied by silver impregnation. *J. Comp. Neurol.* **144**, 215–232.

Iida K., Sasa M., Serikawa T., Noda A., Ishihara K., Akimitsu T., Hanaya R., Arita K. and Kurisu K. (1998) Induction of convulsive seizures by acustic priming in a new genetically defined model of epilepsy (Noda epileptic rat: NER). *Epilepsy Res.* **30**, 115–126.

Iijima T., Witter M. P., Ichikawa M., Tominaga T., Kajiwara R. and Matsumoto G. (1996) Entorhinal–hippocampal interactions revealed by real-time imaging. *Science* **272**, 1176–1179.

Insausti R., Amaral D. G. and Cowan W. M. (1987) The entorhinal cortex of the monkey. III. Subcortical afferents. *J. Comp. Neurol.* **264**, 396–408.

Iwakiri M., Mizukami K., Ishikawa M., Hidaka S. and Asada T. (2002) Alterations of NMDAR1 and NMDAR2A/B immunoreactivity in the hippocampus after perforant path lesion. *Neuropathology* **22**, 154–160.

Jones R. S. G. (1993) Entorhinal–hippocampal connections: a speculative view of their function. *Trends Neurosci.* **16**, 58–64.

Jones R. S. G. and Lambert J. D. C. (1990) The role of excitatory amino acid receptor sin the propagation of epileptiform discharges from the entorhinal cortex to the dentate gyrus *in vitro*. *Exp. Brain Res.* **80**, 310–322.

Jorgensen M. B., Johansen F. F. and Diemer N. H. (1987) Removal of the entorhinal cortex protects hippocampal CA-1 neurons from ischemic damage. *Acta Neuropathol. (Berl.)* **73**, 189–194.

Karnovsky M. J. and Roots L. (1964) A direct-coloring thiocholine method for cholinesterase. *J. Histochem. Cytochem.* **12**, 219–222.

Kloosterman F., Van Haeften T. and Lopes Silva F. H. (2000) Functional characterization of hippocampal output to the entorhinal cortex in the rat. *Ann. NY Acad. Sci.* **911**, 459–461.

Kloosterman F., van Haeften T., Witter M. P. and Lopes da Silva F. H. (2003) Electrophysiological characterization of interlaminar entorhinal connections: an essential link for re-entrance in the hippocampal–entorhinal system. *Eur. J. Neurosci.* **18**, 3037–3052.

Li X.-G., Somogyi P., Ylinen A. and Buzsaki G. (1994) The hippocampal CA3 network: an in vivo intracellular labeling study. *J. Comp. Neurol.* **339**, 181–208.

Mattson M. P., Lee R. E., Adams M. E., Guthrie P. B. and Kater S. B. (1988) Interactions between entorhinal axons and target hippocampal neurons: a role for glutamate in the development of hippocampal circuitry. *Neuron* **1**, 865–876.

Mihály A., Szente M., Dubravcsik Z., Boda B., Kiraly E., Nagy T. and Domonkos A. (1997) Parvalbumin- and calbindin-containing neurons express c-*fos* protein in primary and secondary (mirror) epileptic foci of the rat neocortex. *Brain Res.* **761**, 135–145.

Mihály A., Shihab-Eldeen A., Owunwanne A., Gopinath S., Ayesha A. and Mathew M. (2000) Acute 4-aminopyridine seizures increase the regional cerebral blood flow in the thalamus and neocortex, but not in the entire allocortex of the mouse brain. *Acta Physiol. Hung.* **87**, 43–52.

Mihály A., Szakacs R., Bohata C., Dobo E. and Krisztin-Peva B. (2001) Time-dependent distribution and neuronal localization of c-*fos* protein in the rat hippocampus following 4-aminopyridine seizures. *Epilepsy Res.* **44**, 97–108.

Mihály A., Borbély S., Világi I., Détári L., Weiczner R., Zádor Zs., Krisztin-Péva B., Bagosi A., Kopniczky Z. and Zádor E. (2005) Neocortical c-*fos* mRNA transcription in repeated, brief, acute seizures: is c-*fos* a coincidence detector? *Int. J. Mol. Med.* **15**, 481–486.

Mitchell S. J. and Ranck J. B. Jr (1980) Generation of theta rhythm in medial entorhinal cortex of freely moving rats. *Brain Res.* **189**, 49–66.

Mizukami K., Mishizen A., Ikonovic M. D., Sheffield R. and Armstrong D. M. (1997) Alterations of AMPA-selected glutamate subtype immunoreactivity in the dentate gyrus after perforant pathway lesion. *Brain Res.* **768**, 354–360.

Molnar E. and Isaac J. T. R. (2002) Developmental and activity dependent regulation of ionotropic glutamate receptors at synapses. *Scientificworldjournal* **2**, 27–47.

Molnar E., Varadi A., McIlhinney R. A. J. and Ashcroft S. J. H. (1995) Identification of functional ionotropic glutamate receptor proteins in pancreatic β-cells and islets of Langerhans. *FEBS Lett.* **371**, 253–257.

Molnar E., Pickard L. and Duckworth J. K. (2002) Developmental changes in ionotropic glutamate receptors: Lessons from hippocampal synapses. *Neuroscientist* **8**, 143–153.

Nadler J. V., Cotman C. W. and Lynch G. S. (1977) Histochemical evidence of altered development of cholinergic fibers in the rat dentate gyrus following lesions. I. Time course after complete unilateral entorhinal lesion at various ages. *J. Comp. Neurol.* **171**, 561–588.

Nicolle M. M., Shivers A., Gill T. M. and Gallagher M. (1997) Hippocampal *N*-ethyl-D-aspartate and kainate binding in response to entorhinal cortex aspiration or 192 IgG-saponin lesions of the basal forebrain. *Neuroscience* **77**, 649–659.

Okada M., Zhu G., Yoshida S., Hirose S. and Kaneko S. (2004) Protein kinase associated with gating and closing transmission mechanisms in temporoammonic pathway. *Neuropharmacology* **47**, 485–504.

Paxinos G. and Watson C. (1998) *The Rat Brain in Stereotaxic Coordinates*, 4th edn. Academic Press, San Diego.

Pickard L., Noel J., Henley J. M., Collingridge G. L. and Molnar E. (2000) Developmental changes in synaptic AMPA and NMDA receptor distribution and AMPA receptor subunit composition in living hippocampal neurons. *J. Neurosci.* **20**, 7922–7931.

Raisman G., Cowan W. M. and Powell T. P. S. (1965) The extrinsic afferent, commissural and association fibres of the hippocampus. *Brain* **88**, 963–998.

Rappert A., Bechmann I., Pivneva T. *et al.* (2004) CXCR3-dependent microglial recruitment is essential for dendrite loss after brain lesion. *J. Neurosci.* **24**, 8500–8509.

Reutens D. C. (1999) Entorhinal cortex in temporal lobe epilepsy: a quantitative MRI study. *Neurology* **52**, 1870–1876.

Scharfman H. E. (1996) Hyperexcitability of entorhinal cortex and hippocampus after application of aminooxyacetic acid (AOAA) to layer III of the rat medial entorhinal cortex *in vitro*. *J. Neurophysiol.* **76**, 2986–3001.

Schwarz P., Stichel C. C. and Luhmann H. J. (2000) Characterization of neuronal migration disorders in neocortical structures: loss or preservation of inhibitory interneurons? *Epilepsia* **41**, 781–787.

Sloviter R. S. (1983) 'Epileptic' brain damage in rats induced by sustained electrical stimulation of the perforant path. I. Acute electrophysiological and light microscopic studies. *Brain Res. Bull.* **10**, 675–697.

Steward O. and Scoville S. A. (1976) Cells of origin of entorhinal cortical afferents to the hippocampus and fascia dentata of the rat. *J. Comp. Neurol.* **169**, 347–370.

Stoop R. and Pralong E. (2000) Functional connections and epileptic spread between hippocampus, entorhinal cortex and amygdala in a modified horizontal slice preparation of the rat brain. *Eur. J. Neurosci.* **12**, 3651–3663.

Stringer J. L. and Lothman E. W. (1992) Reverberatory seizure discharges in hippocampal-parahippocampal circuits. *Exp. Neurol.* **116**, 198–203.

Sunanda, Meti B. L. and Raju T. R. (1997) Entorhinal cortex lesioning protects hippocampal CA3 neurons from stress-induced damage. *Brain Res.* **770**, 302–306.

Swanson L. W. and Köhler C. (1986) Anatomical evidence for direct projections from the entorhinal area to the entire cortical mantle in the rat. *J. Neurosci.* **6**, 3010–3023.

Szakács R., Weiczner R., Mihaly A., Krisztin-Peva B., Zador Z. and Zador E. (2003) Non-competitive NMDA receptor antagonists moderate seizure-induced c-*fos* expression in the rat cerebral cortex. *Brain Res. Bull.* **59**, 485–493.

Tago H., Kimura H. and Maeda T. (1986) Visualization of detailed acetylcholinesterase fiber and neuron staining in rat brain by a sensitive histochemical procedure. *J. Histochem. Cytochem.* **34**, 1431–1438.

Tonnes J., Stierli B., Cerletti C., Behrmann J. T., Molnar E. and Streit P. (1999) Regional distribution and developmental changes of GluR1-flop protein revealed by monoclonal antibody in rat brain. *J. Neurochem.* **73**, 2195–2205.

Ułas J., Monaghan D. T. and Cotman C. W. (1990a) Kainate receptors in the rat hippocampus: a distribution and time course of changes in response to unilateral lesions of the entorhinal cortex. *J. Neurosci.* **10**, 2352–2362.

Ułas J., Monaghan D. T. and Cotman C. W. (1990b) Plastic response of hippocampal excitatory amino acid receptors to deafferentation and reinnervation. *Neuroscience* **34**, 9–17.

Weissinger F., Buchheim K., Siegmund H., Heinemann U. and Meierkord H. (2000) Optical imaging reveals characteristic seizure onsets, spread patterns, and propagation velocities in hippocampal-

entorhinal cortex slices of juvenile rats. *Neurobiol. Dis.* **7**, 286–298.

White L. E. and Price J. L. (1993) The functional anatomy of limbic status epilepticus in the rat. II. The effects of focal deactivation. *J. Neurosci.* **13**, 4810–4830.

Wisden W., Seeburg P. H. and Monyer H. (2000) AMPA, kainate and NMDA ionotropic glutamate receptor expression: an in situ hybridization atlas, in Glutamate. Handbook of Chemical Neuroanatomy (Ottersen O. P. and Storm-Mathisen J., *eds)*, Vol. 18, pp. 99–143. Elsevier.

Witter M. P., Naber P. A., van Haeften T., Machielsen W. C., Rombouts S. A., Barkhof F., Scheltens P. and Lopes da Silva F. H. (2000) Cortico-hippocampal communication by way of parallel parahippocampal-subicular pathways. *Hippocampus* **10**, 398–410.

Xu B., McIntyre D. C., Fahnestock M. and Racine R. J. (2004) Strain differences affect the induction of status epilepticus and seizure-induced morphological changes. *Eur. J. Neurosci.* **20**, 403–418.